
PROBLEM REPORT

If you have experienced a problem with the delivery of the requested item, please contact us with the following information. Send back this form via fax or e-mail.

San Jose Library
Interlibrary Services
One Washington Square
San Jose, CA 95192-0028

FAX: 408-808-2078
E-mail: library-ils-group@sjsu.edu

_____ Pages were missing pp. _____ to _____

_____ Edges were cut off pp. _____ to _____

_____ Illegible copy – please resend entire item

_____ Incorrect article sent

_____ Not received

_____ Other (please explain)

Computers & Structures Vol. 23, No. 6, pp. 819–829, 1986
Printed in Great Britain.

0045-7949/86 $3.00 + 0.00
Pergamon Journals Ltd.

NONLINEAR FINITE ELEMENT MODELING OF THE DYNAMICS OF UNRESTRAINED FLEXIBLE STRUCTURES

E. R. CHRISTENSEN† and S. W. LEE‡
Department of Aerospace Engineering, University of Maryland, College Park, MD 20742, U.S.A.

(*Received* 1 *August* 1985)

Abstract—A finite element modeling and solution technique capable of determining the time response of unrestrained flexible structures which are undergoing large elastic deformations coupled with gross nonsteady translational and rotational motions with respect to an inertial reference frame has been developed. The governing equations of motion are derived using momentum conservation principles and the principle of virtual work. The finite element approximation is applied to the equations of motion and the resulting set of nonlinear second order matrix differential equations is solved timewise by a direct numerical integration scheme based on the trapezoidal rule and Newton–Raphson type iterations. The solution technique is tested on some simple structures consisting of long, slender, uniform beams attached to a rigid mass.

1. INTRODUCTION

In order to predict the motion of many types of flexible spacecraft, it is necessary to accurately simulate the time response of an unrestrained structure which is undergoing large elastic deformations as well as gross nonsteady rigid body translations and rotations. For such structures, the large elastic deformations are coupled with the rigid body motions resulting in a complicated set of nonlinear differential equations. Such spacecraft may be simple enough to be modeled as rigid bodies supporting flexible beams or they may be more complicated structures consisting of frames, plates and shells in combination with one or more rigid bodies. If such a spacecraft were to execute a sudden rotational maneuver or reorientation, then large elastic deformations coupled with rigid body motion would occur. An accurate time response analysis of the motion of the structure would be necessary in order to predict the orientation of the structure, especially if it were necessary to determine the pointing accuracy of any sensors which may be attached to the spacecraft.

Extensive research has been done in the dynamics of flexible spacecraft undergoing small elastic deformations. The motion of unrestrained flexible structures has been discussed by Bisplinghoff and Ashley [1], who considered small vibrations of aircraft structures using a modal technique. Ashley [2] also studied gravitational excitation of very simple elastic spacecraft under the restriction of infinitesimal elastic displacements as well as categorizing typical free–free structural configurations according to whether or not the associated nodal generalized forces vanish identically. McDonough [3] considered the formulation of the global equations of motion of an unrestrained deformable body using translating and rotating reference frames but made no attempt at solving them. Fraejis de Veubeke [4] considered the motion of a flexible body undergoing arbitrarily large rotations with respect to an inertial frame. The motion was split into a mean rigid body motion chosen so as to minimize the mean square of relative displacements and a relative motion taking into account the deformations. Kane and Levinson [5] have considered different methods for formulating the equations of motion for complex flexible spacecraft including momentum principles, D'Alembert's principle, and Lagrange's equations, among others. Santini [6] has studied the stability of both nonspinning and spinning flexible spacecraft in a gravitational field by the superposition of a rigid motion plus a combination of structural modes. Meirovitch [7, 8] has developed a method of solution of the eigenvalue problem for gyroscopic systems with applications to spinning spacecraft containing elastic parts. Many other investigators [9–16] have also studied these types of problems using both general analyses or in connection with more specific spacecraft.

The finite element method has also been used to study flexible spacecraft dynamics. Kane and Levinson [17] have developed an algorithm for producing numerical simulations of large motions of a nonuniform flexible cantilever beam in orbit using finite elements. Likins [18] and Tsing [19] have used the finite element method to study spacecraft with flexible appendages. All of these studies, however, have been limited to the case of small deformations. The objective of this paper, therefore, is to develop a finite element method to determine the time response of unrestrained flexible structures which are undergoing large elastic deformations coupled with gross

† Formerly graduate student, now Assistant Professor, Auburn University, AL.
‡ Associate Professor.

nonsteady rigid body translational and rotational motions with respect to an inertial reference. The method developed can be used to study the effects that any large displacements may have on the pointing accuracy and control of various types of spacecraft.

The formulation and solution scheme used for this research can be briefly described as follows. The governing equations of motion are derived using momentum conservation principles and the principle of virtual work. The finite element approximation is applied to the equations of motion and a matrix form of those equations is obtained. The resulting set of nonlinear second order matrix differential equations is solved timewise by a direct numerical time integration scheme based on the trapezoidal rule and Newton–Raphson iteration. The solution technique is tested on simple spacecraft consisting of long slender uniform beams attached to a rigid mass and modeled by three-dimensional beam elements. The effects of inertial forces and control forces on the motion of the spacecraft are considered.

2. EQUATIONS OF MOTION

For elastic structures undergoing gross translational and angular motion as well as small or large deformations the motion can be described by the following three sets of equations:

1. The conservation of linear momentum.
2. The conservation of angular momentum.
3. An equation which describes the deformations of the structure.

If the structure is very flexible, the deformed configuration may be quite different from the undeformed configuration and the deformations will be coupled with the gross translational and rotational motion, especially if the applied loads are deformation or velocity dependent.

2.1. *Geometry and kinematics*

Consider the deformable body pictured in Fig. 1. A set of mutually orthogonal axes, x_1, x_2 and x_3 are fixed in the undeformed body at point 0 which is located a distance $\mathbf{R}_0$ from a set of mutually orthogonal inertial axes, X_1, X_2 and X_3, centered at point C. The body axes are translating with velocity $\mathbf{V}_0$ and rotating with angular velocity $\boldsymbol{\Omega}$ relative to the inertial axes. A point P located a distance $\mathbf{r}_0$ from 0 displaces by $\mathbf{u}$ to point P' as the body deforms so that it is now a distance $\mathbf{r}$ from 0. Point P' is located a distance $\mathbf{R}$ from C, where

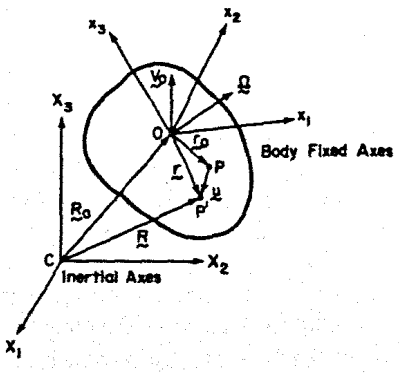

Fig. 1. Reference axis for an unrestrained deformable body.

$$\mathbf{R} = \mathbf{R}_0 + \mathbf{r} = \mathbf{R}_0 + \mathbf{r}_0 + \mathbf{u}. \tag{1}$$

In order to express the motion in terms of the rotating body axes, it is necessary to express the acceleration of point P in terms of body axis coordinates,

$$\frac{d^2\mathbf{R}}{dt^2} = \frac{d\mathbf{V}_0}{dt} + \ddot{\mathbf{r}} - \mathbf{r} \times \dot{\boldsymbol{\Omega}} + 2\boldsymbol{\Omega} \times \dot{\mathbf{r}} + \boldsymbol{\Omega} \times (\boldsymbol{\Omega} \times \mathbf{r}). \tag{2}$$

But

$$\frac{d\mathbf{V}_0}{dt} = \dot{\mathbf{V}}_0 + \boldsymbol{\Omega} \times \mathbf{V}_0 \tag{3}$$

and

$$\dot{\mathbf{r}}_0 = \ddot{\mathbf{r}}_0 = \mathbf{0}. \tag{4}$$

Thus

$$\frac{d^2\mathbf{R}}{dt^2} = \dot{\mathbf{V}}_0 + \boldsymbol{\Omega} \times \mathbf{V}_0 + \ddot{\mathbf{u}} - \mathbf{r} \times \dot{\boldsymbol{\Omega}} + 2\boldsymbol{\Omega} \times \dot{\mathbf{r}} + \boldsymbol{\Omega} \times (\boldsymbol{\Omega} \times \mathbf{r}). \tag{5}$$

In order to simplify eqn (5) a little, the cross products can be replaced by matrix products. If $\mathbf{A}$ and $\mathbf{B}$ are any 3-vectors, then

$$\mathbf{A} \times \mathbf{B} = \bar{\mathbf{A}}\mathbf{B}, \tag{6}$$

where

$$\bar{\mathbf{A}} = \begin{bmatrix} 0 & -A_3 & A_2 \\ A_3 & 0 & -A_1 \\ -A_2 & A_1 & 0 \end{bmatrix}. \tag{7}$$

Note that vector and matrix notation is the same, that is, an n-vector is considered an $n \times 1$ matrix. Using eqn (6) in eqn (5) results in

$$\frac{d^2\mathbf{R}}{dt^2} = \dot{\mathbf{V}}_0 + \bar{\boldsymbol{\Omega}}\mathbf{V}_0 + \ddot{\mathbf{u}} - \bar{\mathbf{r}}\dot{\boldsymbol{\Omega}} + 2\bar{\boldsymbol{\Omega}}\dot{\mathbf{r}} + \bar{\boldsymbol{\Omega}}^2\mathbf{r}. \tag{8}$$

2.2. *Finite element expressions for velocity and acceleration*

The incremental change in displacement during the time increment Δt is represented by $\Delta\mathbf{u}$. In the finite element formulation for large displacement problems the value of $\Delta\mathbf{u}$ within each element is approximated by

$$\Delta\mathbf{u} = \mathbf{N}^* \Delta\mathbf{q}, \tag{9}$$

where $\Delta\mathbf{q}$ is the increment of nodal displacement vector $\mathbf{q}$. The matrix $\mathbf{N}^*$ is composed of the shape functions for the element. For beam, plate and shell elements, $\mathbf{N}^*$ is also a function of the nodal displacements $\mathbf{q}$. The velocity is defined as

$$\dot{\mathbf{u}} = \lim_{\Delta t \to 0} \frac{\Delta \mathbf{u}}{\Delta t} = \lim_{\Delta t \to 0} \mathbf{N}^* \frac{\Delta \mathbf{q}}{\Delta t} = \mathbf{N}^* \dot{\mathbf{q}}, \tag{10}$$

where eqn (9) has been used. Differentiating eqn (10),

$$\ddot{\mathbf{u}} = \mathbf{N}^* \ddot{\mathbf{q}} + \dot{\mathbf{N}}^* \dot{\mathbf{q}} \simeq \mathbf{N}^* \ddot{\mathbf{q}}, \tag{11}$$

where the fact has been used that $\dot{\mathbf{N}}^* \dot{\mathbf{q}}$ is either zero for solid elements or very small in the case of beam, plate or shell elements.

2.3. *Conservation of linear momentum*

If $\mathbf{F}_T$ is the vector sum of the externally applied forces acting on the body of mass density ρ, then conservation of linear momentum requires that

$$\frac{\mathrm{d}}{\mathrm{d}t} \int_V \rho \frac{\mathrm{d}\mathbf{R}}{\mathrm{d}t} \mathrm{d}V = \int_V \rho \frac{\mathrm{d}^2\mathbf{R}}{\mathrm{d}t^2} \mathrm{d}V = \mathbf{F}_T. \tag{12}$$

The integral in eqn (12) is defined over the volume V of the original undeformed configuration. Substituting the expression for the acceleration given in eqn (5) into eqn (12) and using eqns (10) and (11) results in

$$\mathbf{P}^{\mathrm{T}} \ddot{\mathbf{q}} + \mathbf{G}^{\mathrm{T}} \dot{\bar{\mathbf{\Omega}}} + M \mathbf{V}_0 = \mathbf{f}_T, \tag{13}$$

where

$$\mathbf{f}_T = \mathbf{F}_T - M \bar{\mathbf{\Omega}} \mathbf{V}_0 - 2\bar{\mathbf{\Omega}} \mathbf{P}^T \dot{\mathbf{q}} - \mathbf{f}_c, \tag{14}$$

$$M = \int \rho \, \mathrm{d}v = \text{total mass of body}, \tag{15}$$

$$\mathbf{P}^T = \sum_{i=1}^{N} \int_{V_i} \rho \, \mathbf{N}^* \, \mathrm{d}V = \sum_{i=1}^{N} \mathbf{P}_i^T, \tag{16}$$

$$\mathbf{G}^T = -\int_V \rho \, \bar{\mathbf{r}} \, \mathrm{d}V, \tag{17}$$

$$\mathbf{f}_c = \bar{\mathbf{\Omega}}^2 \int_V \rho \mathbf{r} \, \mathrm{d}V. \tag{18}$$

The $\mathbf{P}_i$ matrix is called the element linear momentum matrix. Note that $\mathbf{P}^T$ is the summation or assembly over all N finite elements. The elements of the $\mathbf{G}$ matrix represent the location of the instantaneous center of mass of the body while $\mathbf{f}_c$ is the force at 0 due to the centripetal acceleration.

2.4. *Conservation of angular momentum*

If $\mathbf{M}_T$ is the vector sum of the externally applied moments about the inertial axes, then the conservation of angular momentum requires that

$$\frac{\mathrm{d}}{\mathrm{d}t} \int_V \left(\mathbf{R} \times \frac{\mathrm{d}\mathbf{R}}{\mathrm{d}t} \right) \rho \, \mathrm{d}V = \int_V \left(\mathbf{R} \times \frac{\mathrm{d}^2\mathbf{R}}{\mathrm{d}t^2} \right) \rho \, \mathrm{d}V = \mathbf{M}_T. \tag{19}$$

Substituting eqn (1) into eqn (19) and using eqn (12) results in

$$\mathbf{M}_T = \mathbf{R}_0 \times \mathbf{F}_T + \int_V \rho \left(\mathbf{r} \times \frac{\mathrm{d}^2\mathbf{R}}{\mathrm{d}t^2} \right) \mathrm{d}V. \tag{20}$$

If $\mathbf{M}_0$ represents the vector sum of externally applied moments about the body axes, then

$$\mathbf{M}_T = \mathbf{M}_0 + \mathbf{R}_0 \times \mathbf{F}_T. \tag{21}$$

Thus eqn (20) reduces to

$$\mathbf{M}_0 = \int_V \rho \left(\mathbf{r} \times \frac{\mathrm{d}^2\mathbf{R}}{\mathrm{d}t^2} \right) \mathrm{d}V. \tag{22}$$

Substituting eqn (5) into eqn (22) and using eqns (15)–(18) results in

$$\mathbf{H}^T \ddot{\mathbf{q}} + \mathbf{I}_T \dot{\bar{\mathbf{\Omega}}} + \mathbf{G} \mathbf{V}_0 = \mathbf{m}_T, \tag{23}$$

where

$$\mathbf{m}_T = \mathbf{M}_0 - \mathbf{G} \bar{\mathbf{\Omega}} \mathbf{V}_0 - \mathbf{M}_{\mathrm{cor}} - \mathbf{M}_{\mathrm{cent}}, \tag{24}$$

$$\mathbf{I}_T = -\int_V \rho \, \bar{\mathbf{r}}^2 \, \mathrm{d}V, \tag{25}$$

$$\mathbf{H}^T = \sum_{i=1}^{N} \int_{V_i} \rho \, \bar{\mathbf{r}} \mathbf{N}^* \, \mathrm{d}V = \sum_{i=1}^{N} \mathbf{H}_i^T, \tag{26}$$

$$\mathbf{M}_{\mathrm{cor}} = 2 \int_V \rho \bar{\mathbf{r}} \bar{\mathbf{\Omega}} \dot{\mathbf{u}} \, \mathrm{d}V, \tag{27}$$

$$\mathbf{M}_{\mathrm{cent}} = \int_V \rho \bar{\mathbf{r}} \bar{\mathbf{\Omega}}^2 \mathbf{r} \, \mathrm{d}V. \tag{28}$$

The $\mathbf{I}_T$ matrix represents the instantaneous moment of inertia matrix of the entire structure. The $\mathbf{H}_i$ matrix is called the element angular momentum matrix. The $\mathbf{M}_{\mathrm{cor}}$ and $\mathbf{M}_{\mathrm{cent}}$ vectors represent moments about 0 due to the Coriolis and centrifugal forces, respectively.

2.5. *Deformation equation*

The deformations of the body are described using the principle of virtual work,

$$\int_V \delta \mathbf{E}^T \mathbf{S} \, \mathrm{d}V - \int_V \delta \mathbf{u}^T \mathbf{F} \, \mathrm{d}V - \int_{S\sigma} \delta \mathbf{u}^T \bar{\mathbf{T}} \, \mathrm{d}S = 0. \tag{29}$$

The first integral in eqn (29) represents the virtual work done by the internal forces, where $\mathbf{S}$ is the column vector of second Pyola–Kirchhoff stresses

and $\delta\mathbf{E}$ is the column vector of virtual Green strains,

$$\mathbf{S}^T = \lfloor S_{11}\, S_{22}\, S_{33}\, S_{12}\, S_{13}\, S_{23} \rfloor, \tag{30}$$

$$\delta\mathbf{E}^T = \lfloor \delta E_{11}\, \delta E_{22}\, \delta E_{33}\, 2\delta E_{12}\, 2\delta E_{13}\, 2\delta E_{23} \rfloor. \tag{31}$$

The second integral represents the virtual work of the body forces $\mathbf{F}$ including the inertia force. The third integral is the virtual work of the surface tractions $\mathbf{T}$ which are applied over S_σ.

First, consider the second integral in eqn (29). The body forces are

$$\mathbf{F} = -\rho \frac{\mathrm{d}^2\mathbf{R}}{\mathrm{d}t^2} + \mathbf{F}_b, \tag{32}$$

where the first term in egn (32) represents the inertia force and $\mathbf{F}_b$ represents any other applied body forces. If eqn (32) is substituted into eqn (29) and if eqns (5), (10), (11), (15)–(17) and (26) are used, then the second integral in eqn (29) becomes as follows for the i^{th} element

$$-\int_{V_i} \delta\mathbf{u}^T\mathbf{F}\,\mathrm{d}V = \delta\mathbf{q}^T(\mathbf{M}\ddot{\mathbf{q}} + \mathbf{H}\dot{\boldsymbol{\Omega}} + \mathbf{P}\dot{\mathbf{V}}_0 + \mathbf{C}_G\dot{\mathbf{q}} + \mathbf{P}\bar{\boldsymbol{\Omega}}\mathbf{V}_0 + \mathbf{F}_c - \mathbf{F}_B), \tag{33}$$

where

$$\mathbf{M} = \int_{V_i} \rho\, \mathbf{N}^{*T}\mathbf{N}^*\,\mathrm{d}V, \tag{34}$$

$$\mathbf{C}_G = 2\int_{V_i} \rho\mathbf{N}^{*T}\bar{\boldsymbol{\Omega}}\mathbf{N}^*\,\mathrm{d}V, \tag{35}$$

$$\mathbf{F}_c = \int_{V_i} \rho\mathbf{N}^{*T}\bar{\boldsymbol{\Omega}}^2\mathbf{r}\,\mathrm{d}V, \tag{36}$$

$$\mathbf{F}_B = \int_{V_i} \mathbf{N}^{*T}\mathbf{F}_b\,\mathrm{d}V. \tag{37}$$

The $\mathbf{M}$ matrix is the consistent mass matrix and $\mathbf{C}_G$ is the gyroscopic matrix, which is skew-symmetric and represents the contribution of the Coriolis acceleration to the nodal inertia force. The $\mathbf{F}_c$ vector is the nodal force vector due to the centrifugal force and $\mathbf{F}_B$ is the force due to any other applied body forces. Note that the volume integrals are evaluated over the original undeformed volume.

The third integral in eqn (29) is treated in the standard fashion for finite elements,

$$\int_{S_\sigma} \delta\mathbf{u}^T\bar{\mathbf{T}}\,\mathrm{d}S = \delta\mathbf{q}^T\mathbf{F}_0, \tag{38}$$

where $\mathbf{F}_0$ is the vector of applied forces at the nodes which result from the applied tractions.

Now, applying the finite element approximation to the first integral in eqn (29) results in [20]

$$\int_{V_i} \delta\mathbf{E}^T\mathbf{S}\,\mathrm{d}v = \delta\mathbf{q}^T\mathbf{F}_E(\mathbf{q}), \tag{39}$$

where $\mathbf{F}_E$ is the elastic force vector and is a nonlinear function of the nodal displacements.

Assembling the element matrices in the usual way and combining eqns (33), (38) and (39) and noting that $\delta\mathbf{q}$ is arbitrary results in the deformation equation

$$\mathbf{M}\ddot{\mathbf{q}} + \mathbf{H}\dot{\boldsymbol{\Omega}} + \mathbf{P}\dot{\mathbf{V}}_0 + \mathbf{F}_E(\mathbf{q}) = \mathbf{F}_q, \tag{40}$$

where

$$\mathbf{F}_q = \mathbf{F}_0 + \mathbf{F}_B - \mathbf{F}_C - \mathbf{P}\bar{\boldsymbol{\Omega}}\mathbf{V}_0 - \mathbf{C}_G\dot{\mathbf{q}}. \tag{41}$$

Thus eqns (13), (23) (40) are the three sets of nonlinear coupled equations of motion for the unrestrained deformable system of Fig. 1.

3. NUMERICAL TIME INTEGRATION SCHEME

There are many methods which can be used for the numerical time integration of eqns (13), (23) and (40). Generally speaking, these methods can be classified as either explicit or implicit schemes [23–25]. Explicit schemes are computationally simple but the time step size is limited by stability considerations. Implicit schemes require more computation per time step, but time step size limitations are much less stringent. The type of element used here results in stiff systems with widely varying natural frequencies necessitating the use of very small time steps in any explicit scheme. Therefore an implicit scheme based on the trapezoidal rule has been used.

To facilitate the discussion of the numerical integration scheme, eqns (13), (23) and (40) are written in a more compact form by writing the three equations as a single "generalized" matrix equation,

$$\mathbf{M}_G\ddot{\mathbf{q}}_G + \mathbf{F}_{GE}(\mathbf{q}_G) = \mathbf{F}_G, \tag{42}$$

where

$$\mathbf{q}_G = \begin{Bmatrix} \mathbf{q} \\ \mathbf{d} \\ \boldsymbol{\phi} \end{Bmatrix}, \tag{43}$$

$$\mathbf{M}_G = \begin{bmatrix} \mathbf{M}(\mathbf{q}) & \mathbf{P}(\mathbf{q}) & \mathbf{H}(\mathbf{q}) \\ \mathbf{P}^T(\mathbf{q}) & M\mathbf{I}_3 & \mathbf{G}(\mathbf{q}) \\ \mathbf{H}^T(\mathbf{q}) & \mathbf{G}^T(\mathbf{q}) & \mathbf{I}_T(\mathbf{q}) \end{bmatrix}, \tag{44}$$

$$\mathbf{F}_{GE} = \begin{Bmatrix} \mathbf{F}_E(\mathbf{q}) \\ \mathbf{0} \\ \mathbf{0} \end{Bmatrix}, \tag{45}$$

$$\mathbf{F}_G = \begin{Bmatrix} \mathbf{F}_q(\mathbf{q}_G, \dot{\mathbf{q}}_G) \\ \mathbf{f}_T(\mathbf{q}_G, \dot{\mathbf{q}}_G) \\ \mathbf{m}_T(\mathbf{q}_G, \dot{\mathbf{q}}_G) \end{Bmatrix}, \tag{46}$$

$$\dot{\mathbf{d}} = \mathbf{V}_0, \tag{47}$$

$$\dot{\boldsymbol{\phi}} = \boldsymbol{\Omega}. \tag{48}$$

$\mathbf{I}_3$ is the 3×3 identity matrix and $\mathbf{0}$ represents a null matrix. Assuming all the variables in eqn (42) are known at time t_n, the equation at time $t_{n+1} = t_n + \Delta t$ is

$$\mathbf{M}_G^{n+1}\ddot{\mathbf{q}}_G^{n+1} + \mathbf{F}_{GE}^{n+1} = \mathbf{F}_G^{n+1} \tag{49}$$

where

$$\mathbf{q}_G^{n+1} = \mathbf{q}_G(t_{n+1}), \tag{50}$$

$$\mathbf{M}_G^{n+1} = \mathbf{M}_G(\mathbf{q}_G^{n+1}), \tag{51}$$

$$\mathbf{F}_{GE}^{n+1} = \mathbf{F}_{GE}(\mathbf{q}_G^{n+1}), \tag{52}$$

$$\mathbf{F}_G^{n+1} = \mathbf{F}_G(\mathbf{q}_G^{n+1}, \dot{\mathbf{q}}_G^{n+1}). \tag{53}$$

The trapezoidal rule for this problem is

$$\mathbf{q}_G^{n+1} = \mathbf{q}_G^n + \frac{\Delta t}{2}(\dot{\mathbf{q}}_G^n + \dot{\mathbf{q}}_G^{n+1}), \tag{54}$$

$$\dot{\mathbf{q}}_G^{n+1} = \dot{\mathbf{q}}_G^n + \frac{\Delta t}{2}(\ddot{\mathbf{q}}_G^n + \ddot{\mathbf{q}}_G^{n+1}). \tag{55}$$

Combining eqns (54) and (55) results in

$$\ddot{\mathbf{q}}_G^{n+1} = \frac{4}{(\Delta t)^2}(\mathbf{q}_G^{n+1} - \mathbf{q}_G^n) - \frac{4}{\Delta t}\dot{\mathbf{q}}_G^n - \ddot{\mathbf{q}}_G^n. \tag{56}$$

Substituting eqn (56) into eqn (42) yields

$$\mathbf{M}_G^{n+1}\left[\frac{4}{(\Delta t)^2}(\mathbf{q}_G^{n+1} - \mathbf{q}_G^n) - \frac{4}{\Delta t}\dot{\mathbf{q}}_G^n - \ddot{\mathbf{q}}_G^n\right] + \mathbf{F}_{GE}(\mathbf{q}_G^{n+1}) = \mathbf{F}_G^{n+1}. \tag{57}$$

Equation (57) is a nonlinear equation and can be solved by Newton–Raphson iteration. Letting subscript i represent the i^{th} iteration number, eqn (57) becomes, for $i = 1, 2, \ldots,$

$$\mathbf{M}_{G_i}^{n+1}\left[\frac{4}{(\Delta t)^2}(\mathbf{q}_{G_{i+1}}^{n+1} - \mathbf{q}_G^n) - \frac{4}{\Delta t}\dot{\mathbf{q}}_G^n - \ddot{\mathbf{q}}_G^n\right] + \mathbf{F}_{GE}(\mathbf{q}_{G_{i+1}}^{n+1}) = \mathbf{F}_{G_i}^{n+1}. \tag{58}$$

But

$$\mathbf{F}_{GE}(\mathbf{q}_{G_{i+1}}^{n+1}) = \mathbf{K}_{GT_i}^{n+1}\Delta\mathbf{q}_{G_i}^{n+1} + \mathbf{F}_{GS_i}^{n+1}, \tag{59}$$

where

$$\Delta\mathbf{q}_{G_i}^{n+1} = \mathbf{q}_{G_{i+1}}^{n+1} - \mathbf{q}_{G_i}^{n+1}, \tag{60}$$

$$\mathbf{K}_{GT_i}^{n+1} = \begin{bmatrix} \mathbf{K}_T(\mathbf{q}_{G_i}^{n+1}) & \mathbf{0} & \mathbf{0} \\ \mathbf{0} & \mathbf{0} & \mathbf{0} \\ \mathbf{0} & \mathbf{0} & \mathbf{0} \end{bmatrix}, \tag{61}$$

$$\mathbf{F}_{GS_i}^{n+1} = \begin{Bmatrix} \mathbf{F}_S(\mathbf{q}_{G_i}^{n+1}) \\ \mathbf{0} \\ \mathbf{0} \end{Bmatrix}. \tag{62}$$

$\mathbf{K}_T$ is called the tangential stiffness matrix and $\mathbf{F}_S$ is the initial stress force vector [20]. After using eqn (59) and rearranging a few terms, eqn (58) becomes

$$\mathbf{K}_{G_i}^{*}\Delta\mathbf{q}_{G_i}^{n+1} = \mathbf{F}_{G_i}^{n+1} - \mathbf{F}_{GS_i}^{n+1} - \mathbf{M}_{G_i}^{n+1}\ddot{\mathbf{q}}_{G_i}^{n+1}, \tag{63}$$

where

$$\mathbf{K}_{G_i}^{*} = \mathbf{K}_{GT_i}^{n+1} + \frac{4}{(\Delta t)^2}\mathbf{M}_{G_i}^{n+1}. \tag{64}$$

To start the iterations ($i = 0$), the state of the structure at time t_n is used as a first approximation to the state of the structure at time t_{n+1} for all the terms except $\mathbf{F}_{G_i}^{n+1}$, that is,

$$\mathbf{q}_{G_0}^{n+1} = \mathbf{q}_G^n, \tag{65}$$

$$\mathbf{M}_{G_0}^{n+1} = \mathbf{M}_G^n, \tag{66}$$

$$\mathbf{K}_{GT_0}^{n+1} = \mathbf{K}_{GT}^n, \tag{67}$$

$$\mathbf{F}_{GS_0}^{n+1} = \mathbf{F}_{GS}^n. \tag{68}$$

Note that when eqn (65) is used in eqn (56),

$$\ddot{\mathbf{q}}_{G_0}^{n+1} = -\frac{4}{\Delta t}\dot{\mathbf{q}}_G^n - \ddot{\mathbf{q}}_G^n. \tag{69}$$

The mass and stiffness matrices change slowly enough with time so that eqn (65) is good enough for a first iteration of those terms. Since $\mathbf{F}_{G_i}^{n+1}$ is a nonlinear function of both $\mathbf{q}_{G_i}^{n+1}$ and $\dot{\mathbf{q}}_{G_i}^{n+1}$, however, a better predictor for this term is given by [26]

$$\tilde{\dot{\mathbf{q}}}_{G_0}^{n+1} = \mathbf{q}_G^n + \left(\frac{\Delta t}{2}\right)\ddot{\mathbf{q}}_G^n, \tag{70}$$

$$\tilde{\mathbf{q}}_{G_0}^{n+1} = \mathbf{q}_G^n + \Delta t\,\dot{\mathbf{q}}_G^n + \frac{(\Delta t)^2}{4}\ddot{\mathbf{q}}_G^n, \tag{71}$$

where the upper tilde indicates a quantity used in calculating $\mathbf{F}_{G_0}^{n+1}$. Note that eqns (70) and (71) are obtained by setting $\ddot{\mathbf{q}}_G^{n+1} = 0$ in eqns (54) and (55).

For subsequent iterations ($i > 0$), the displacements, velocities and accelerations are "corrected" using eqns (54)–(56),

$$\mathbf{q}_{G_i}^{n+1} = \mathbf{q}_{G_{i-1}}^{n+1} + \Delta\mathbf{q}_{G_{i-1}}^{n+1}, \tag{72}$$

$$\dot{\mathbf{q}}_{G_i}^{n+1} = \dot{\mathbf{q}}_{G_{i-1}}^{n+1} + \frac{2}{\Delta t}\Delta\mathbf{q}_{G_{i-1}}^{n+1}, \tag{73}$$

$$\ddot{\mathbf{q}}_{G_i}^{n+1} = \ddot{\mathbf{q}}_{G_{i-1}}^{n+1} + \frac{4}{(\Delta t)^2}\Delta\mathbf{q}_{G_{i-1}}^{n+1}. \tag{74}$$

$\mathbf{K}_G^{*}$ and the right-hand side of eqn (63) can now be recomputed using eqns (72)–(74). The iterations continue until $\Delta\mathbf{q}_{G_i}^{n+1}$ converges to within a required tolerance, i.e. until

$$\left\| \frac{\Delta\mathbf{q}_{G_i}^{n+1}}{\mathbf{q}_{G_i}^{n+1} - \mathbf{q}_G^n} \right\| \leq \text{Tol}, \tag{75}$$

where $\|\cdot\|$ is a given vector norm and Tol is the tolerance. For the problems considered here, Tol = 0.01.

The regular Newton–Raphson iteration scheme used here could be replaced by a modified Newton–Raphson iteration in whch the $\mathbf{K}_G^*$ matrix is kept constant throughout the iterations. However, a larger number of iterations will generally be necessary.

4. THE THREE NODE EIGHTEEN DEGREE OF FREEDOM BEAM ELEMENT

The equations developed in Section 2 will in general apply to any type of element. For the example problems discussed in this paper, however, the three node eighteen degree of freedom beam element is used. For this element, large deflections and rotations are allowed but the strains are assumed to remain small. Transverse shear is allowed but there is no warping of the cross-section. Each element is assumed to be uniform with constant cross-sectional area.

For this three node element, the element stiffness matrix is developed using the Lagrangian description in which all variables are referred to the original undeformed configuration. If $\mathbf{a}_1$, $\mathbf{a}_2$, $\mathbf{a}_3$ are a set of mutually orthogonal unit vectors located at the centroid of the undeformed cross-section with $\mathbf{a}_1$ tangent to the beam axis, then as the beam deforms these vectors translate and rotate to new positions $\mathbf{a}_1'$, $\mathbf{a}_2'$, $\mathbf{a}_3'$ which remain mutually orthogonal as shown in Fig. 2. The vectors $\mathbf{a}_1'$, $\mathbf{a}_2'$, $\mathbf{a}_3'$ are functions of both the position along the beam as well as the rotation angles. Because plane sections remain plane during the deformation, $\mathbf{a}_2'$ and $\mathbf{a}_3'$ remain in the cross-sectional plane and the displacement of any point in the cross-section can be expressed as

$$\mathbf{u} = \mathbf{u}_0 + (\mathbf{a}_2' - \mathbf{a}_2)\zeta_2 + (\mathbf{a}_2' - \mathbf{a}_3)\zeta_3, \tag{76}$$

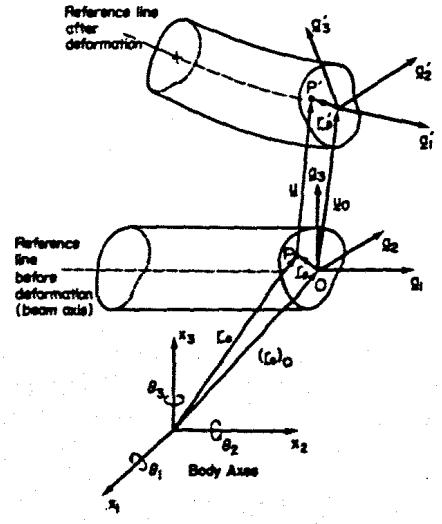

Fig. 2. Beam undergoing large displacement.

where $\mathbf{u}_0$ is the displacement of the centroid and ζ_2 and ζ_3 are the coordinates of the point in the cross-section. In order to relate $\mathbf{a}_1'$, $\mathbf{a}_2'$, $\mathbf{a}_3'$ to $\mathbf{a}_1$, $\mathbf{a}_2$, $\mathbf{a}_3$, a way of describing the rotations must be found. There are many well known ways of doing this, probably the best known way being Euler angles. Another way is by the use of space-three or body-three angles [21], which consist of successive rotations about space or body axes. For this element, a space-three: 1–2–3 description was used which consisted of successive rotations of θ_1, θ_2 and θ_3 about the original $\mathbf{a}_1$, $\mathbf{a}_2$, $\mathbf{a}_3$ axes to transform then to the $\mathbf{a}_1'$, $\mathbf{a}_2'$, $\mathbf{a}_3'$ axes. The vectors $\mathbf{a}_1'$, $\mathbf{a}_2'$, $\mathbf{a}_3'$ can then be expressed as functions of $\theta_1, \theta_2, \theta_3$ and $\mathbf{a}_1, \mathbf{a}_2, \mathbf{a}_3$,

$$\mathbf{a}_k' = f_k(\theta_1, \theta_2, \theta_3, \mathbf{a}_1, \mathbf{a}_2, \mathbf{a}_3), \quad K = 1, 2, 3, \tag{77}$$

where f_k is the transformation function. Next the displacements and rotations are written in an incremental form

$$\mathbf{u}_0 = {}^\circ\mathbf{u}_0 + \Delta\mathbf{u}_0, \tag{78}$$

$$\theta_k = {}^\circ\theta_k + \Delta\theta_k, \qquad k = 1, 2, 3, \tag{79}$$

where ${}^\circ\mathbf{u}_0$ and ${}^\circ\theta_k$ are the displacement and rotation at time t_n and $\Delta\mathbf{u}_0$ and $\Delta\theta_k$ are the incremental displacements and rotations. Using eqns (77)–(79) in eqn (76) and neglecting second order terms in $\Delta\mathbf{u}_0$ and $\Delta\theta_k$ results in

$$\mathbf{u} = {}^\circ\mathbf{u} + \Delta\mathbf{u} \tag{80}$$

where

$${}^\circ\mathbf{u} = {}^\circ\mathbf{u}_0 + \zeta_2({}^\circ\mathbf{a}_2' - \mathbf{a}_2) + \zeta_3({}^\circ\mathbf{a}_3' - \mathbf{a}_3), \tag{81}$$

$$\Delta\mathbf{u} = \Delta\mathbf{u}_0 + [\zeta_2\mathbf{T}_2({}^\circ\theta_1, {}^\circ\theta_2, {}^\circ\theta_3) + \zeta_3\mathbf{T}_3({}^\circ\theta_1, {}^\circ\theta_2, {}^\circ\theta_3)]\Delta\boldsymbol{\theta}, \tag{82}$$

$$\Delta\boldsymbol{\theta}^T = [\Delta\theta_1\Delta\theta_2\Delta\theta_3]. \tag{83}$$

The vectors ${}^\circ\mathbf{a}_2'$ and ${}^\circ\mathbf{a}_3'$ are the values of $\mathbf{a}_2'$ and $\mathbf{a}_3'$ at time t_n and are functions of ${}^\circ\theta_1, {}^\circ\theta_2, {}^\circ\theta_3$. The 3×3 matrices $\mathbf{T}_2$ and $\mathbf{T}_3$ are also functions of ${}^\circ\theta_1, {}^\circ\theta_2, {}^\circ\theta_3$. If the local beam coordinates $\zeta_1, \zeta_2, \zeta_3$ are normalized such that the origin is at the center node of the element and ζ_1 varies between -1 at one end of the element and $+1$ at the other end, then the body axis coordinates of a point in the undeformed beam element are

$$\mathbf{r}_0 = \sum_{i=1}^{3} \mathbf{N}_i(\zeta_1)(\mathbf{r}_0)_{0i} + \zeta_2\mathbf{a}_2 + \zeta_3\mathbf{a}_3, \tag{84}$$

where $(\mathbf{r}_0)_{0i}$ are the body axis coordinates of the three nodes and $\mathbf{N}_i(\zeta_1)$ are the element shape functions. An isoparametric finite element approximation is made in which the displacements are assumed in terms of

the shape functions as

$$^{\circ}\mathbf{u} = \sum_{i=1}^{3} \mathbf{N}_i(\zeta_1)[^{\circ}\mathbf{u}_{oi} + \zeta_2(^{\circ}\mathbf{a}_2' - \mathbf{a}_2)_i + \zeta_3(^{\circ}\mathbf{a}_3' - \mathbf{a}_3)_i], \quad (85)$$

$$\Delta\mathbf{u} = \sum_{i=1}^{3} \mathbf{N}_i(\zeta_1)[\Delta\mathbf{u}_{oi} + (\zeta_2\mathbf{T}_{2i} + \zeta_3\mathbf{T}_{3i})\Delta\theta_i], \quad (86)$$

where the i subscript indicates that the quantity is evaluated at the ith node. If the nodal incremental displacement vector is defined as

$$\Delta\mathbf{q}^T = [\Delta\mathbf{u}_{01}^T\ \Delta\theta_1^T\ \Delta\mathbf{u}_{02}^T\ \Delta\theta_2^T\ \Delta\mathbf{u}_{03}^T\ \Delta\theta_3^T] \quad (87)$$

then using eqn (86), the N^* matrix in eqn (9) can be written as

$$\mathbf{N}^* = \mathbf{N}_0^* + \zeta_2\mathbf{N}_2^* + \zeta_3\mathbf{N}_3^*, \quad (88)$$

where

$$\mathbf{N}_0^* = [N_1\mathbf{I}_3\mathbf{0}\,N_2\mathbf{I}_3\mathbf{0}\,N_3\mathbf{I}_3\mathbf{0}], \quad (89)$$

$$\mathbf{N}_k^* = [\mathbf{0}N_1\mathbf{T}_{k1}\,\mathbf{0}N_2\mathbf{T}_{k2}\mathbf{0}N_3\mathbf{T}_{k3}], \quad k = 2, 3. \quad (90)$$

Note that $\mathbf{N}_0^*$, $\mathbf{N}_2^*$ and $\mathbf{N}_3^*$ are 3×18 matrices since $\mathbf{I}_3$ is the 3×3 identity matrix and $\mathbf{0}$ is the 3×3 null matrix.

Using the expressions in eqns (85) and (86), the various derivatives and integrals used in calculating the element tangential stiffness matrix and initial stress force vector can then be evaluated. To eliminate shear locking, 2-point Gaussian integration was used to evaluate integrals along the length of the beam. The details of all the calculations are given in Ref. [22].

5. NUMERICAL RESULTS

The use of the method developed in the previous sections will now be illustrated by some example problems which utilize the three node beam element of Section 4.

5.1. *A beam rotating about a fixed axis*

As shown in Fig. 3, a thin uniform flexible beam is fixed to a shaft which is rotating about its centerline with an angular velocity $\Omega(t)$. The beam has a length $L = 100$ ft and cross-sectional properties $A = 1$ ft^2, $I_{\zeta_2\zeta_2} = I_{\zeta_3\zeta_3} = 0.08333$ ft^4. It is made of a fictitious material with mass density $\rho = 5.22$ slug/ft^3, Young's modulus $E = 1.44(10^8)$ lb/ft^2, and shear modulus $G_S = 5.54(10^7)$ lb/ft^2. The shaft has a mass moment of inertia of I_R about its centerline which is fixed so that no translations can occur. The mass moment of inertia of the undeformed beam about the rotation axis is I_B. The radius r_c of the shaft is considered negligible compared to the length of the beam. A set of body axes x_1, x_2 and x_3 are fixed in the shaft and rotate with it. At time $t = 0$ the beam and the shaft are at rest with the beam centerline along the x_1 axis.

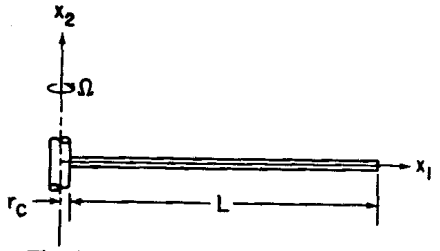

Fig. 3. Beam rotating about a fixed axis.

In part one of this example, it is desired to determine the deflections of the beam given the angular velocity $\Omega(t)$ as a function of time for all time. The only unknowns are the nodal displacements and velocities which can be found using eqn (40) with $\mathbf{V}_0 = \dot{\mathbf{V}}_0 = \mathbf{0}$ and $\mathbf{\Omega}(t)$ and $\dot{\mathbf{\Omega}}(t)$ given. Note that specifying $\mathbf{\Omega}(t)$ implies that a moment is applied to turn the shaft. This moment can be determined by solving for $\mathbf{M}_0(t)$ in eqn (23).

For the second part of this example, the angular velocity is specified only for $t \le T_{\text{MOM}}$ after which it becomes an unknown variable due to the applied moment being released. The time period $0 \le t \le T_{\text{MOM}}$ is the "spin-up" period during which the beam is accelerated from rest to a given angular velocity. The motion is the same as for part one during the spin-up period but for $t \ge T_{\text{MOM}}$ eqn (23) must be solved simultaneously with eqn (40) with $\mathbf{M}_0 = \mathbf{0}$ since Ω is unknown for this time period. For each of the two cases the angular velocity during spin-up is a smooth polynomial.

Case 1. $\Omega(t)$ *specified for all time*

$$\Omega(t) = \begin{cases} \Omega_0\left[6\left(\dfrac{t}{T_0}\right)^5 - 15\left(\dfrac{t}{T_0}\right)^4 + 10\left(\dfrac{t}{T_0}\right)^3\right], & 0 \le t \le T_0, \\ \Omega_0, & t \ge T_0. \end{cases} \quad (91)$$

Case 2. $\Omega(t)$ *unknown for* $t \ge T_{\text{MOM}}$

$$\Omega(t) = \begin{cases} \Omega_0\left[6\left(\dfrac{t}{T_0}\right)^5 - 15\left(\dfrac{t}{T_0}\right)^4 + 10\left(\dfrac{t}{T_0}\right)^3\right], & 0 \le t \le T_0, \\ \Omega_0, & T_0 \le t \le T_{\text{MOM}}, \\ \text{Unknown variable } (M_0 = 0), & t > T_{\text{MOM}}. \end{cases} \quad (92)$$

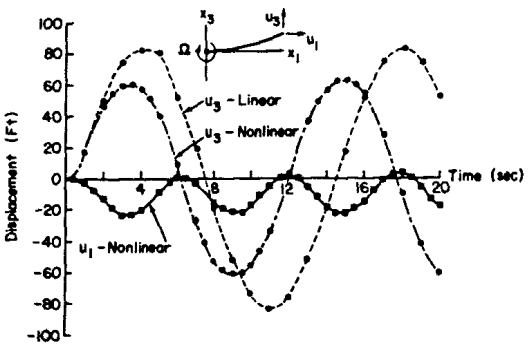

Fig. 4. Tip displacement of a rotating beam.

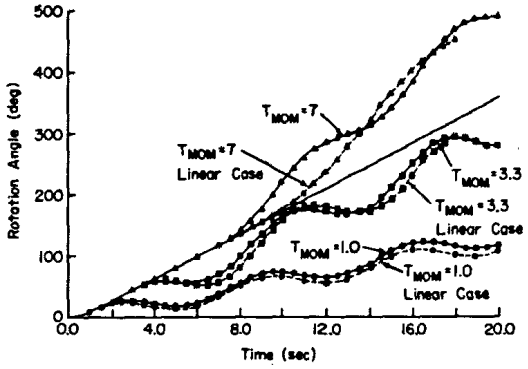

Fig. 6. Body axis rotation angle ($I_R/I_B = 0.5$).

For both cases, values of $\Omega_0 = \pi/10$ rad/sec and $T_0 = 1$ sec were used. The equations of motion were integrated using a time step of $\Delta t = 0.1$ sec and one beam element was used.

The results for case 1 are shown in Figs. 4 and 5. Figure 4 is a plot of the beam tip displacements versus time for both large displacement theory as well as linear beam theory. In Fig. 5 is pictured the orientation of the deformed beam at various times. The dashed lines represent the positions of the x_1 body axis at the given times and coincide with the motion of a rigid beam. The solid lines represent the shapes of the deformed beam with the arrows representing the tip displacements.

The errors that can result from using linear beam theory when large displacements occur are evident from Fig. 4. The linear theory indicates maximum lateral displacements about 35% greater than the actual displacements as well as predicting almost zero axial displacements. Also, the linear theory predicts a natural frequency of vibration for the beam of $\omega = 0.433$ rad/sec compared to $\omega = 0.524$ rad/sec from nonlinear theory.

The results for case 2 are presented in Figs 6–7, which present a plot of the rotation angle of the body axes for $T_{MOM} = 1.0$, 3.3 and 7.0 sec with $I_R/I_B = 0.5$ in Fig. 6 and $I_R/I_B = 1.0$ in Fig. 7. The actual rotations are compared to the rigid body case in both figures and to linear beam theory in Fig. 6. For both of the inertia ratios, the "average" angular velocity of the body axes is greater than Ω_0 for $T_{MOM} = 7$ and less than Ω_0 for $T_{MOM} = 1.0$, while for $T_{MOM} = 3.3$ it is about the same as Ω_0. All the angular velocities are closer to Ω_0 for the larger inertia ratio in Fig. 7 than in Fig. 6. Finally, note that the longer the moment is applied to the shaft, the greater the difference between the linear and nonlinear solutions.

In order to understand the behavior of the beam in Figs 6 and 7, consider what happens when the moment support is released at $t = T_{MOM}$ and the angular velocity becomes a free variable. For $t > T_{MOM}$, the angular momentum of the system is constant

$$\mathbf{H}_A = \int_V \rho\left(\mathbf{r} \times \frac{\mathrm{d}\mathbf{r}}{\mathrm{d}t}\right) \mathrm{d}V = \text{const.} \tag{93}$$

But

$$\frac{\mathrm{d}\mathbf{r}}{\mathrm{d}t} = \boldsymbol{\Omega} \times \mathbf{r} + \dot{\mathbf{u}}. \tag{94}$$

Substituting eqns (94) and (10) into eqn (93) and using eqns (25) and (26) results in

$$\mathbf{H}_A = \mathbf{I}_T \boldsymbol{\Omega} + \mathbf{H}^T \dot{\mathbf{q}}. \tag{95}$$

For this particular problem, $\mathbf{H}_A$, $\mathbf{I}_T$ and $\boldsymbol{\Omega}$ are scalars and

$$I_T = I_R + I_B. \tag{96}$$

Also, let

$$H_D = \mathbf{H}^T \dot{\mathbf{q}}. \tag{97}$$

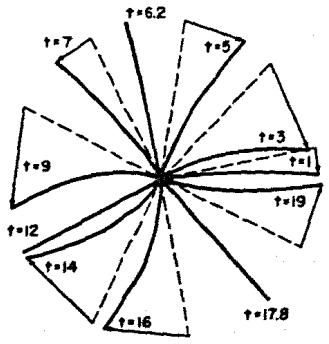

Fig. 5. Large displacements of a rotating beam.

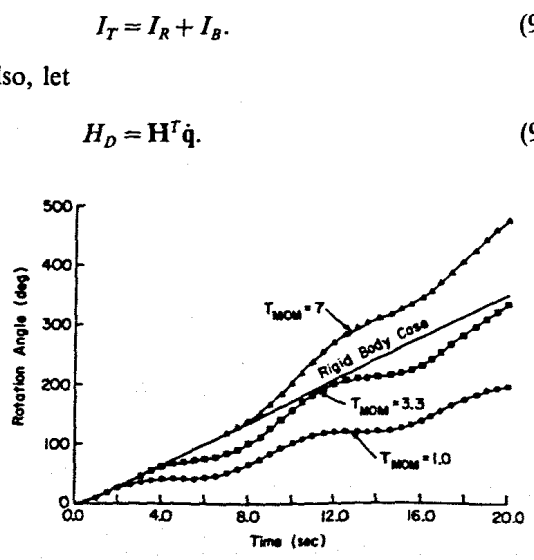

Fig. 7. Body axis rotation angle ($I_R/I_B = 1.0$).

The value of I_B will change only slightly as the beam vibrates and for the purposes of this discussion it is sufficient to consider it to be a constant. The conservation of angular momentum requires that

$$(I_R + I_B)\Omega_0 + H_{D_0} = (I_R + I_B)\Omega + H_D, \quad (98)$$

where

$$H_{D_0} = (H_D)_{t = T_{MOM}}. \quad (99)$$

Solving for Ω,

$$\Omega = \Omega_0 + \left(\frac{1}{I_R + I_B}\right)(H_{D_0} - H_D). \quad (100)$$

Taking a time average of eqn (100),

$$\Omega_{Avg} = \Omega_0 + \left(\frac{1}{I_R + I_B}\right)[H_{D_0} - (H_D)_{Avg}]. \quad (101)$$

Since the beam vibrates about the x_1 axis, the average of H_D over a given cycle will be small and can be neglected. Thus,

$$\Omega_{Avg} \simeq \Omega_0 + \left(\frac{1}{I_R + I_B}\right) H_{D_0}. \quad (102)$$

So if

$$H_{D_0} < 0, \quad \text{then } \Omega_{Avg} < \Omega_0, \quad (103)$$

$$H_{D_0} = 0, \quad \text{then } \Omega_{Avg} = \Omega_0, \quad (104)$$

$$H_{D_0} > 0, \quad \text{then } \Omega_{Avg} > \Omega_0. \quad (105)$$

Also, the larger I_R is in comparison to I_B, the closer Ω_{Avg} will be to the rigid body velocity Ω_0.

Now eqn (102) can be used to explain the behavior of the beam in Figs 6 and 7. At $t = 1.0$ sec the beam is moving away from the body axis and thus $H_{D_0} < 0$. At $t = 3.3$ sec the beam has reached its maximum displacement relative to the body axis and thus $H_{D_0} \simeq 0$. At $t = 7.0$ sec the beam is "leading" the rigid body motion and $H_{D_0} > 0$. Thus the average angular velocities pictured in Fig. 6 are as predicted by eqn (102). Similar results are obtained in Fig. 7 except that, with a larger inertia ratio, all the average angular velocities are closer to Ω_0 as predicted by eqn (102).

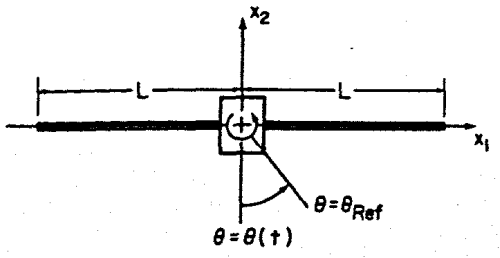

Fig. 8. Spacecraft rotating to a specified orientation.

Finally, from Fig. 4 note that at $t = 7.0$ sec the difference between the linear and nonlinear solution is greater than the difference at $t = 1.0$ or 3.3 sec. This would also account for the fact that the error between the linear and nonlinear solutions in Fig. 6 is greater for $T_{MOM} = 7.0$ sec.

5.2. A spacecraft rotating to a specified orientation

In this example the simple dipole spacecraft pictured in Fig. 8 consisting of two beams attached to a rigid mass is rotated through a specified angle by a control moment which is applied at the center of the rigid mass

$$M_0 = -K_s(\theta - \theta_{Ref}) - K_w\Omega, \quad (106)$$

where K_S and K_w are control constants and θ_{Ref} is the reference angle through which the spacecraft is to be rotated. The beams have the following properties: $L = 50$ ft, $A = 0.02182$ ft^2, $I_{\zeta_2\zeta_2} = I_{\zeta_3\zeta_3} = 3.0419\ (10^{-4})$ ft^4, $\rho = 5.22$ slug/ft^3, $E_0 = 1.44(10^8)$ lb/ft^3 and $G_{S_0} = 5.54(10^7)$ lb/ft^3. The properties of the rigid mass are total mass $m_R = 50$ slugs, moment of inertia $I_{11} = I_{22} = 10^3$ slug-ft^2 and $I_{33} = 2.5(10^3)$ slug-ft^2. If a sensor or some other instrument for which pointing accuracy is important is attached to the spacecraft, it is necessary to know how $\theta(t)$ varies with time.

The rigid body solution for this problem is the response typical of underdamped second order control systems,

$$\theta_{Rigid} = \theta_{Ref}\left\{1 - e^{-\xi_d\omega t}\left[\cos\omega_d t + \frac{\xi_d}{\sqrt{1-\xi_d^2}}\sin\omega_d t\right]\right\}, \quad (107)$$

where

$$\omega = \sqrt{K_s/I_{33}}\text{: undamped natural frequency,} \quad (108)$$

$$\xi_d = K_w/2\omega I_{33}\text{: damping constant,} \quad (109)$$

$$\omega_d = \omega\sqrt{1-\xi_d^2}\text{: damped natural frequency.} \quad (110)$$

I_{33} is the spacecraft mass moment of inertia about the symmetry axis. If p is the desired percent overshoot of the response and t_r the desired rise time, then

$$\xi_d^2 = \left(\frac{\ln^2 p}{\pi^2 + \ln^2 p}\right), \quad (111)$$

$$\omega t_r = \frac{1}{\sqrt{1-\xi_d^2}}\left[\text{Tan}^{-1}\left(-\frac{\sqrt{1-\xi_d^2}}{\xi_d}\right) + \pi\right]. \quad (112)$$

Using values of $p = 0.01$ and $t_r = 5$ sec results in $I_{33} = 15{,}122$ slug-ft^2, $K_S = 12{,}316$ ft-lb/rad and $K_w = 22{,}547$ ft-lb-sec. A value of $\theta_{Ref} = 20°$ was chosen as the reference angle.

Since the spacecraft is symmetric, only half of it need be modeled. The motion was studied using both

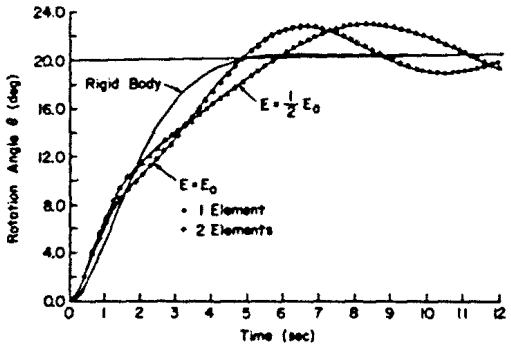

Fig. 9. Body axis rotating angle θ.

one and two beam elements with a time step size of $\Delta t = 0.1$ sec. In addition, two values of Young's modulus were used. The results for both the rigid body and elastic rotation angles are pictured in Fig. 9. Note that for $E = E_0$, the peak overshoot is near 10% and it takes more than 12 sec before θ does not vary more than 1% from 20°. The more flexible beam with $E = \frac{1}{2} E_0$ still has a peak overshoot of 10% but it takes even longer for the rotation to settle down to within 1% of θ_{Ref}. Large lateral displacements of the beam tips of up to 22% of the beam length occur and are plotted in Fig. 10.

6. CONCLUSIONS

A solution technique capable of determining the time response of unrestrained flexible structures which are undergoing large elastic deformations coupled with gross nonsteady rigid body translational and rotational motions with respect to an inertial reference has been developed. The numerical results clearly indicate that the deflections of the structure do have a substantial effect on the motion and that the effects of large displacements cannot be ignored.

Although only beam elements have been used in this work, the equations in Section 2 are general and will apply for more complicated elements such as plates and shells. In addition to developing more complex elements, future work along the lines of this research could also investigate different types of materials including composites. Problems which include thermal effects such as solar heating could be studied. Also, more complicated types of motion such as spacecraft deployment problems involving rotations and relative velocities between different spacecraft parts could be studied.

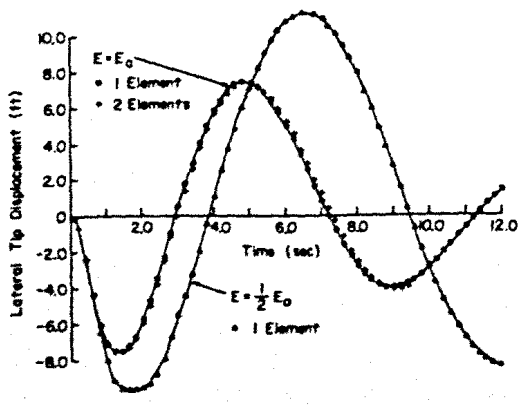

Fig. 10. Beam tip displacements.

Acknowledgement—The present work was supported by AFOSR (Grant No. AFOSR-82-0296) with Dr. A. K. Amos as the program monitor.

REFERENCES

1. H. Ashley and R. L. Bisplinghoff, *Principles of Aeroelasticity*. John Wiley, New York (1962).
2. H. Ashley, Observations on the dynamic behavior of large flexible bodies in orbit, *AIAA J.* **5**, 460–469 (1967).
3. T. B. McDonough, Formulation of the global equations of motion of a deformable body. *AIAA J.* **14**, 656–660 (1976).
4. B. Fraejis de Veubeke, The dynamics of flexible bodies. *Int. J. Engng Sci.* **14**, 895–913 (1976).
5. T. R. Kane and D. A. Levinson, Formulation of equations of motion for complex spacecraft. *J. Guidance Control* **3**, 99–112 (1980).
6. P. Santini, Stability of flexible spacecraft. *Acta Astron.* **3**, 685–731 (1976).
7. L. Meirovitch, A new method of solution of the eigenvalue problem for gyroscopic systems, *AIAA J.* **12**, 1337–1342 (1974).
8. L. Meirovitch, A stationarity principle for the eigenvalue problem for rotating structures. *AIAA J.* **14**, 1387–1394 (1976).
9. J. K. Newton and J. L. Farrell, Natural frequencies of a flexible gravity-gradient satellite. *J. Spacecraft Rockets* **5**, 560–569 (1968).
10. P. B. Grote, J. C. McMunn and R. Gluck, Equations of motion of flexible spacecraft. *J. Spacecraft Rockets* **8**, 561–567 (1971).
11. V. K. Kumar and P. M. Bainum, Dynamics of a flexible body in orbit. *J. Guidance Control* **3**, 90–91. (1980).
12. R. Sellapan and P. M. Bainum, Modal control of the planar motion of a long flexible beam in orbit. *Acta Astron.* **7**, 19–36 (1980).
13. R. M. Davis, K. Yong and W. E. Blair, Dynamic behavior of an extremely flexible gravity-gradient dipole satellite. AAS Paper No. 75-091 (1975).
14. D. R. Smart, K. F. Gill, J. M. Gething and J. A. Holt, Dynamic analysis of flexible space vehicles having uncoupled control axes. *Aeronaut. J.*, 560–569 (December 1974).
15. F. Austin and H. H. Pan, Planar dynamics of free rotating beams with tip masses. *AIAA J.* **8**, 726–733 (1970).
16. P. C. Hughes, Attitude dynamics of a three-axis stabilized satellite with a large flexible solar array. *J. Astron. Sci.* **XX**, 166–189 (1972).
17. T. R. Kane and D. A. Levinson, Simulation of large motions of nonuniform beams in orbit. *J. Astron. Sci.* **29**, 213–244 (1981).
18. P. W. Likins, Finite element appendage equations for hybrid coordinate dynamic analysis. *Int. J. Solids Struct.* **8**, 709–731 (1972).
19. G. T. Tsing, Dynamical equations of spacecraft with controlled flexible appendages using finite element approach. AIAA Paper No. 74-1261 (October 1974).
20. O. C. Zienkiewicz, *The Finite Element Method in Engineering Science*. McGraw-Hill, New York (1971).
21. T. R. Kane, P. W. Likins and D. A. Levinson, *Spacecraft Dynamics*. McGraw-Hill, New York (1983).

22. E. R. Christensen, Development of a dynamic finite element model for unrestrained flexible structures, Ph.D. dissertation, University of Maryland (1984).
23. G. L. Goudreau and R. L. Taylor, Evaluation of numerical integration methods in elastodynamics. *Comput. Meth. appl. Mech. Engng* **2**, 69–97 (1972).
24. C. A. Felippa and K. C. Park, Direct time integration methods in nonlinear structural dynamics. *Comput. Meth. appl. Mech. Engng* **17**, 277–313.
25. J. F. McNamara, Solution schemes for problems of nonlinear structural dynamics. *J. Pressure Vessel Technol.*, 96–102 (May 1974).
26. T. J. R. Hughes, K. S. Pister and R. L. Taylor, Implicit–explicit finite elements in nonlinear transient analysis. *Comput. Meth. appl. Mech. Engng* **17/18**, 159–182 (1979).